Acta Chemica Scandinavica, 1999: 53: 1043–1053
Printed in UK. All rights reserved

ACTA
CHEMICA SCANDINAVICA
ISSN 0904–213X

Dynamical Model for S_N2 Reactions in Microsolution: The $Cl^- + CH_3Cl \rightarrow CH_3 + Cl^-$ Reaction. Molecular Dynamics Simulation of Reaction Clusters

Thomas Nymand,[a] Kurt V. Mikkelsen,[b,*] Per-Olof Åstrand[b] and Gert D. Billing[b]

[a]Department of Chemistry, Aarhus University, Århus, Denmark and [b]Department of Chemistry, University of Copenhagen, Copenhagen, Denmark

Dedicated to Professor Henning Lund on the occasion of his 70th birthday

Nymand, T., Mikkelsen, K. V., Åstrand, P.-O. and Billing, G. D., 1999. Dynamical Model for S_N2 Reactions in Microsolution: The $Cl^- + CH_3Cl \rightarrow CH_3 + Cl^-$ Reaction. Molecular Dynamics Simulation of Reaction Clusters. – Acta Chem. Scand. 53: 1043–1053. © Acta Chemica Scandinavica 1999.

A dynamical model for chemical reactions in microsolution is investigated. The reacting system is enclosed in a cluster of solvent molecules and the dynamics of the reaction is monitored by solving the classical equations of motion for the system consisting of reacting and solvent molecules. The rate constant is calculated as a function of the number of solvent molecules and temperature. In order to achieve a better understanding of the cluster structure and its dynamical properties, molecular dynamics simulations have been performed. These show that water clusters have rather different properties – structural as well as dynamical – from liquid water.

Chemical reactions in solution differ significantly from gas-phase reactions.[1] The presence of a surrounding medium can drastically modify the potential surface along the reaction coordinate and the solvent molecules can participate in the dynamic processes. The influence of the medium may be understood qualitatively by describing it as a dielectric medium, and by realizing that polar species are stabilized to a greater extent by the medium than less polar species. Nonetheless, direct interactions (e.g., hydrogen bonds) may drastically disturb this picture. On the other hand, there is little knowledge about how the surrounding molecules affect the detailed dynamics of chemical reactions in solution. One reason for this is the difficulty associated with obtaining good intermolecular potentials. In simulations of pure water,[2–3] it has been demonstrated that, while static properties such as liquid structure are relatively easy to model, dynamic properties are much more sensitive to the potential. Another reason is the fact that a large number of solvent molecules must be included in the model to give a good description of the surrounding liquid.

The substitution nucleophilic bimolecular, S_N2, or unimolecular, S_N1 reaction mechanisms suggested by Hughes, Ingold and Patel have spurred substantial research activity (see Refs. 4–8). Recently new branches have been formed, namely the exciting discoveries of a rather continuous transition from an electron transfer mechanism to a substitution nucleophilic reaction mechanism.[9]

In the gas phase many S_N2 reactions have been investigated and comparisons with similar reactions in solution have revealed differences in the rate constants of several orders of magnitude.[1] Theoretical investigations of S_N2 reactions in solution have focused on explaining these differences and in most cases the investigated reaction has been eqn. (1)

$$Cl'^- + CH_3Cl \rightarrow Cl'CH_3 + Cl^- . \quad (1)$$

Recently full multidimensional potential energy functions for the reaction have been established.[10–14] Prior to this the methyl group has generally been treated as a single body in the intermolecular potential. In this work we present the effect of microsolvation on the reaction in eqn. (1) using molecular dynamics and calculating the rate constants according to the procedure in Ref. 13.

Microsolvated systems play an important role in the chemistry of the atmosphere.[15] Furthermore they allow for a systematic approach for investigating how the solvent influences the dynamics of chemical reactions.

* To whom correspondence should be addressed.

What follows is an investigation of a dynamic model for microsolvation of a reacting system. The interaction between the solvent and the reactants is modeled with an intermolecular potential and the dynamics of the solvent are included by classical molecular dynamics simulations. The rate constants are calculated as a function of the number of solvent molecules and one point of interest is to compare these with the bulk rate constant, which we have calculated previously.[13] The thermodynamic average of any classical observable, $\langle A \rangle$, may in the canonical ensemble be obtained as[16]

$$\langle A \rangle = \frac{\int d\Gamma A(\Gamma) e^{-H(\Gamma)/kT}}{\int d\Gamma e^{-H(\Gamma)/kT}}, \tag{2}$$

where Γ is a point in the phase space and the integrations are performed over the entire phase space. Applying eqn. (2) to reactive flux, and introducing the 'no recrossing' approximation yields the well known rate constant of transition state theory (TST),[17] eqn. (3),

$$k_{TST} = \frac{\int_{p_s>0} \Pi\, dp_j\, dq_j (p_s/m_s)\delta(s) e^{-H(\{p_j,q_j\})/kT}}{(1/V)\int \Pi\, dp_j\, dq_j e^{-H(\{p_j,q_j\})/kT}}, \tag{3}$$

where $H(\{p_j, q_j\})$ is the classical Hamiltonian for the system, and s is the reaction coordinate. The dividing surface is assumed to be at $s=0$ and $\{p_j, q_j\}$ is the set of coordinates, q_j, and their conjugated momenta, p_j. A dynamic correction to the rate constant may be obtained by calculating the transmission factor, $\langle \xi \rangle$, as the fraction of reactive trajectories and using it as a scaling factor[18,19]

$$k = \langle \xi \rangle k_{TST}. \tag{4}$$

It has been argued[18,19] that this combined phase space–trajectory method is equivalent to a conventional trajectory method, i.e. the only assumption is that of classical mechanics. This assumption does not present serious problems, since the relatively heavy masses of the reacting species diminish the tunneling effect.[14]

Interaction potentials

The system considered in the calculations consists of $3N+6$ atoms, where N is the number of water molecules in the cluster. The equations of motion are governed by the potential and Newton's equations. The potential has been given in detail elsewhere[13] and will be sketched only briefly here. The multidimensional potential energy functions have been shown to be of sufficiently high accuracy for considering chemical reactions.[10–14]

The total potential energy V_{total} may be divided into

$$V_{total} = V_r + V_s + V_{sr} + V_{ind}. \tag{5}$$

where V_r accounts for the interactions between atoms belonging to the reactant system $ClCH_3Cl^-$, V_s is the potential describing the solvent, V_{sr} deals with interactions between the reactant system and the solvent molecules and V_{ind} is the many-body induction energy. The potential is extensively parametrized and a complete list of parameters and their values are given elsewhere.[13]

The potential for the reactant system. The atoms in the reactant system are labeled as follows. The chlorine atoms are denoted 1 and 3, the carbon atom 2 and the hydrogen atoms are referred to by 4–6. The configuration of the saddle point (the van der Waal structure) is denoted sad (vdW). The potential for the reactant system is composed of the elements as given in eqn. (6),

$$V_r = V_{LEPS} + V^r_{ele} + V^r_{intra}, \tag{6}$$

where V_{LEPS} (LEPS: London–Eyring–Polanyi–Sato) denotes the reactive part of the potential, V^r_{ele} the electrostatic part and V^r_{intra} describes the intramolecular motion. V_{LEPS} is a function of the three distances r_{12}, r_{23} and r_{13}, where a distance between atoms i and j is denoted by r_{ij}. $V_{LEPS}(r_{12}, r_{23}, r_{13})$ thus describes the three particle system Cl–C–Cl and it is given by

$$V_{LEPS} = Q_{12} + Q_{23} + Q_{13} - \sqrt{\tfrac{1}{2}[(J_{12}-J_{23})^2 + (J_{23}-J_{13})^2 + (J_{13}-J_{12})^2]}. \tag{7}$$

where

$$Q_{ij} = \frac{1}{2}\left({}^1V_{ij} + \frac{1-\Delta_{ij}}{1+\Delta_{ij}}{}^3V_{ij}\right) \tag{8}$$

and

$$J_{ij} = \frac{1}{2}\left({}^1V_{ij} - \frac{1-\Delta_{ij}}{1+\Delta_{ij}}{}^3V_{ij}\right). \tag{9}$$

The singlet and triplet curves, ${}^1V_{ij}$ and ${}^3V_{ij}$, are approximated by Morse and anti-Morse potentials, respectively, and the Sato parameters, Δ_{ij}, are further parametrized.[13]

The electrostatic contribution to the interaction is calculated as a Coulomb interaction, eqn. (10),

$$V^r_{ele} = \sum_{i,j>i} \frac{q_i q_j}{r_{ij}} f^2(r_{ij}), \tag{10}$$

where q_i is the partial charge at atom i. The switching function $f(r)$ has been introduced to make the internal Coulomb interaction vanish when the chloride ion has moved to infinity and is given by eqn. (11),

$$f(r) = \tfrac{1}{2}\{1 + \tanh[a^r(r - d^r_c)]\}, \tag{11}$$

where

$$a^r = a\, e^{\Delta r_c^4}. \tag{12}$$

The cut-off distance, d^r_c, is calculated as shown in eqns. (13) and (14),

$$d^r_c = R_0 - R_1 w(r_c) \tag{13}$$

$$w(r_c) = e^{-\Delta_a r_c^4}. \tag{14}$$

Note that $w(r_c)$ varies with the reaction coordinate, $r_c = r_{12} - r_{23}$, i.e. the asymmetric stretching mode. The charges on the nuclei are also functions of the reaction coordinate. The charges on the chlorine atoms are given by eqn. (15),

$$q_{1,3} = -1.0 + 0.39\{1 + [g(r_{13})(\pm r_c - \bar{r}_c)]\}, \tag{15}$$

where the minus sign is assigned to chlorine atom 1, the plus sign to chlorine atom 3 and

$$g(r_{13}) = g_a(1 - e^{-br_{13}^2}). \tag{16}$$

The charge on the carbon atom is given by

$$q_2 = q_c e^{-\alpha r_c^2} - 0.389 \tag{17}$$

and on the hydrogen atoms by

$$q_j = \tfrac{1}{3}(\bar{q} - q_2) \quad (j = 4, 5, 6), \tag{18}$$

where $\bar{q}$ is the net charge at the methyl group

$$\bar{q} = -1 - q_1 - q_3. \tag{19}$$

The final term in the reactant potential is the term describing the vibrational degrees of freedom. In this approach the symmetry of the reactant system is automatically built in, leading to a reduction in the number of parameters. The force field expression is given by eqn. (12)

$$\begin{aligned} V_{\text{intra}}^{\text{r}} = {} & \overbrace{\frac{1}{2}\sum_{i=4}^{6} K_i(r_c)(r_{2i} - r_{2i}^0)^2}^{\text{C–H stretch}} + \overbrace{\frac{1}{2}\sum_{i=4,j<i}^{i=6} F_{ij}(r_c)(q_{ij} - q_{ij}^0)^2}^{\text{H–H repulsion}} \\ & + \underbrace{f(r_{13})D_e(r_c)\left(3 - \sum_{i=4,j=1,3}^{i=6} e^{-a\rho_{ij}}[1 + a\rho_{ij} + w(r_c)b\rho_{ij}^2]\right)}_{\text{Asymptotical H–Cl repulsion in } CH_3Cl} \\ & + \overbrace{\frac{1}{2}\sum_{i=4,i<j}^{i=6} G_{ij}(r_c)r_{i2}r_{j2}(\alpha - \alpha_{eq})}^{\text{H–C–H bending}} + \overbrace{\frac{1}{2}\sum_{i=4,j=1,3}^{i=6} w_j H_{ij}(r_c)r_{i2}r_{j2}(\theta - \theta_j)^2}^{\text{H–C–Cl bending}} \\ & + \underbrace{E(r_c)(\gamma - \pi)^2}_{\text{Cl–C–Cl bending}} + \underbrace{L(r_c)\sum_{i=1,3}(r_{i2} - r^*)^2}_{\text{C–Cl stretch near saddle point}} \end{aligned} \tag{20}$$

where

$$K_i(r_c) = K_0 + K_1 w(r_c) \quad (i = 4, 5, 6) \tag{21}$$

$$F_{ij}(r_c) = F_0 + F_1 w(r_c) \quad (i \text{ and } j = 4, 5, 6) \tag{22}$$

$$H_{ij}(r_c) = H_0 + H_1 e^{-0.13r_c^2} \quad (i \text{ and } j = 4, 5, 6) \tag{23}$$

$$G_{ij}(r_c) = G_0 + G_1 w(r_c) \quad (i = 4, 5, 6 \text{ and } j = 1, 2, 3) \tag{24}$$

$$E(r_c) = E_1 w(r_c) \tag{25}$$

$$L(r_c) = L_1 w(r_c) e^{-0.045r_c^4} \tag{26}$$

$$w_1 = \tfrac{1}{2}[1 + \tanh(0.001r_c^3)] \tag{27}$$

$$w_3 = 1 - w_1 \tag{28}$$

and

$$D_e(r_c) = D_e^0 + D_e^1 w(r_c). \tag{29}$$

The parameters introduced are obtained by fitting *ab initio* points as described previously.[13]

Solvent–solvent interactions. The water–water interaction is approximated by the polarizable SPC potential[20] with an additional intramolecular part. Apart from the induction term, it is given as eqn. (30).

$$V_s = V_{LJ}^s + V_{ele}^s + V_{intra}^s. \tag{30}$$

The first term is a Lennard-Jones potential, eqn. (31)

$$V_{LJ}^s = \sum_{i,j>i} \frac{A_{ij}}{r_{ij}^{12}} - \frac{B_{ij}}{r_{ij}^6}, \tag{31}$$

where A_{ij} and B_{ij} depend only on the types of atom i and j. The second term is a screened electrostatic potential similar to eqn. (10)

$$V_{ele}^s = \sum_{i,j>i} \frac{\hat{q}_i\hat{q}_j}{r_{ij}}, \tag{32}$$

where the screened charges are given as eqn. (33)

$$\hat{q}_i = \tfrac{1}{2}q_i\{1 + [a^s(r_{ij} - d_c^s)]\}. \tag{33}$$

This screening was not done in Ref. 20. Note that the effect of this screening is to cut off the Coulomb interaction between molecules very close to each other (d_c^s has the numerical value 0.5).

In order to obtain the total potential for the solvent molecules we add an intramolecular potential describing the vibrations of the water molecule. The atoms of a water molecule are labeled in the following manner: hydrogen atoms are denoted by 1 and 3 and the oxygen atom by 2. By r_{ij}^k we mean the distance between atoms i and j within water molecule k. Then we write the intramolecular potential as eqn. (34),[13]

$$V_{intra}^s = \sum_i [V_{OH}(r_{12}^i) + V_{OH}(r_{23}^i) + V_b(\theta_i)], \tag{34}$$

where the potential of the bond stretching, V_{OH}, is given by a Morse-potential and the potential of the bending motion, V_b, is described within the harmonic approximation.

Solvent–solute interactions. The potential of the interaction between a single water molecule and the $ClCH_3Cl^-$ system is given as eqn. (35),

$$V_{sr} = V_{rep}^{sr} + V_{LJ}^{sr} + V_{ele}^{sr}, \tag{35}$$

where the repulsion term is given as eqn. (36)

$$V_{rep}^{sr} = \sum_{i=1,3}\sum_{j=1,2,3} A_{ij} e^{-a_{ij}r_{ij}}, \tag{36}$$

where i denotes an atom in the reactant system and j denotes an atom in the water molecule, respectively. The Lennard–Jones term is calculated as

$$V_{LJ}^{sr} = \sum_{i=2,4,5,6} \sum_{j=1,2,3} \left(\frac{C_{ij}}{r_{ij}^{12}} - \frac{D_{ij}}{r_{ij}^{6}} \right) \tag{37}$$

and the electrostatic term as

$$V_{ele}^{sr} = \sum_{i,j>i} \frac{q_i(r_c, r_{13}) q_j}{r_{ij}}. \tag{38}$$

Parameters are as given in Refs. 21 and 22.

Many-body induction terms. The induction term V_{ind} is calculated as

$$V_{ind} = -\frac{1}{2} \sum \mu_i E_i^0, \tag{39}$$

where E_i^0 is the electric field from the partial charges and where μ_i, the induced moment at atom i, is given as eqn. (40)

$$\mu_i = \alpha_i (E_i^0 + E_i^{ind}). \tag{40}$$

In this work we neglect the induced field E_i^{ind} and calculate the induction energy as

$$V_{ind} = -\frac{1}{2} \sum \alpha_i E_i^0 \cdot E_i^0. \tag{41}$$

The polarizability of the methyl group is assumed to be given by the polarizability on the carbon atom, $\alpha_2 = \alpha_{CH_3}$, and thus that no contributions arise from the hydrogen atoms in the reactant system. Furthermore, the three polarizabilities in the reactant system are allowed to vary with the charges, and thereby with the reaction coordinate as

$$\alpha_i = \bar{\alpha}_{i0} + \bar{\alpha}_{i1} q_i, \tag{42}$$

where q_2 here is given by $\bar{q}$ as defined in eqn. (19), and the polarizabilities for the water molecules are as given in Ref. 20.

Calculation details

The calculations were initiated by equilibrating the water system later used as the solvent. A molecular dynamics (MD) simulation of 512 water molecules was performed at 300 K using the MOLSIM package.[23] An experimental density of 1.00 g cm^{-3} is used, which corresponds to a box length of 24.8 Å. Periodic boundary conditions were utilized with a cut-off distance of 12.4 Å. Then a radius of about half the box length used in the MD simulation – the largest possible leading to a homogeneous sphere – was chosen. All molecules with the oxygen atom inside the sphere were then used in a further equilibration of a water drop. A reactant box was chosen by adding 1/2 the van der Waals' water–water bond distance to the size of the $ClCH_3Cl$ complex in the sad and vdW states. The configuration of the saddle point (the van der Waal structure) is denoted sad (vdW). The structures of the $ClCH_3Cl$ complex were taken from the previous gas phase calculations.[14] The water molecules in the box (again determined by the position of the oxygen atoms) were removed in order to make room for the reactant system. The system, consisting of 300 water molecules and the fixed reactant system in the vdW configuration, was then equilibrated for 0.5 ps using a timestep of 0.05 fs. Forces were calculated analytically separately from those forces arising from V_{intra}^{r} for which a finite difference method was employed. The calculations were carried out within a parallel computer environment, leading to eight different water structures. These were used as initial water structures for the last equilibration done before the Monte Carlo integration over the momentum space as described in the next section.

Cluster radii were then chosen in order to include a specific number of water molecules. Next, the equations of motion for all particles were solved again while keeping the reactant atoms fixed. In addition the vdW system was allowed to relax after the initial water relaxation, but relaxation is of course allowed for the sad configuration. After the relaxation procedure the temperature can be defined from the average kinetic energy of the water molecules. This temperature was used when evaluating the phase space integral subject to the constraints below using the Monte Carlo technique. In order to obtain an ensemble average the procedure was repeated with a different choice of initial momenta for the water molecules.

These calculations have been implemented to run in a parallel environment. The repetitive nature of the calculations offers the possibility of distributing the work done with each initiated configuration to different processors. The work consists of four main parts: (i) the initial water relaxation, (ii) the optional vdW relaxation, (iii) the integral evaluation and finally (iv) the calculation of the transmission factor. Parts (i) to (iii) perform very well within the distributed model – each task (i), (ii) or (iii) has exactly the same workload for each configuration. Only in (iv) does some workload imbalancing occur but this is acceptable since part (iv) contributes only about 1/5–1/6 to the total workload. A calculation of the speed-up obtained by parallelizing the code has been done, and the result can be seen in Fig. 1. Note that the program runs very well in parallel with an almost linear speed-up.

Calculations of rate constants

The phase space integrals in eqn. (3) were obtained by utilizing the Monte Carlo method[24] and the transmission factor, $\langle \xi \rangle$, is calculated by studying trajectories initiated at the transition state (sad). We followed the procedure described in Ref. 13 where it is clearly stated and shown how this method enables the calculation of rate constants. The Monte Carlo method introduces the concept of importance sampling. In short this means that an ensemble average is obtained by considering a relatively

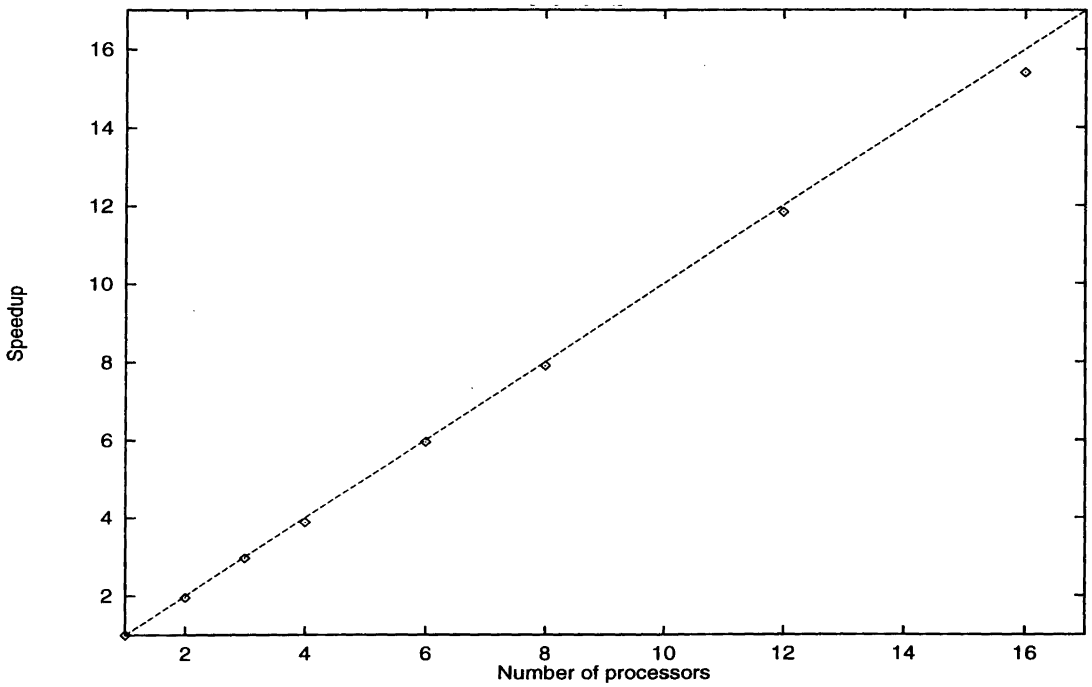

Fig. 1. Parallel speed-up of a vdW calculation on an IBM-SP2 architecture.

small number of important phase points and averaging over these. In the coordinate part of phase space, probable points were obtained by initializing the dynamic system randomly (giving the particles randomly chosen velocities) and equilibrating the system by solving the classical equations of motion over a time period of 20 ps. The temperature of the system eliminates the possible trapping of the system in local minima. When the system was equilibrated, the kinetic energy defined the temperature used to average over the momentum space. When evaluating an integral at the transition state, we also had to subject the system to the constraint that the reactant system is fixed in this position during the equilibration. Finally, we initialized the asymmetric mode of the transition state complex with some momentum, and followed the system to determine whether we had a reactive trajectory or not.

This procedure was repeated for each cluster size. An interpolation procedure gave the integrals as functions of temperature, and the transmission factor was evaluated. Finally rate constants as functions of cluster size and temperature were calculated. Thus, the reaction rate constant was calculated as[18]

$$k = \langle \xi \rangle \frac{1}{Q} \int_{p_{\text{asym}}>0} \Pi \, \mathrm{d}p_j \, \mathrm{d}q_j \frac{p_{\text{asym}}}{m_{\text{asym}}} \times \delta(r_2 - r_1) \, \mathrm{e}^{-H(\{p_j,q_j\})/kT}, \tag{43}$$

where Q is the partition function per unit volume of the reactants, eqn. (44), evaluated at the van der Waals position with $V = \frac{4}{3}\pi R^3_{\text{cluster}}$. In eqn. (43), p_{asym} is the momentum for the asymmetric stretch mode (asym) which for the linear complex is the reactive motion and m_{asym} is the corresponding mass. The phase space integral was subjected to the constraint that $p_{\text{asym}} > 0$ and $r_1 = r_2$ at the dividing surface, i.e. $r_c = 0$. Treatment of Cl^-CH_3Cl as a linear complex along the z axis, so that $m_{\text{sym}} = \frac{1}{2}m_{\text{Cl}}$ and $m_{\text{asym}} = \frac{1}{2}[1 + (2m_{\text{Cl}}/m_{\text{CH}_3})]$ and selecting p_{asym} and p_{sym} from Maxwell distributions, led to the initial Cartesian momenta for the two chlorine and the carbon atoms.[13]

$$Q = \frac{1}{V} \int \Pi \, \mathrm{d}p_j \, \mathrm{d}q_j \, \mathrm{e}^{-H(\{p_j,q_j\})/kT} \tag{44}$$

Calculations with 3, 6, 9, 11, 12, 14, 16, 21 and 30 water molecules were carried out. Up to 128 calculations for each initial water structure and reactant configuration (sad and vdW) were performed leading to a total number of 2048 equilibrations and integrations for each number of solvent molecules. An interpolation was been done for the sad and vdW points to obtain an analytical expression for the configuration integrals as functions of temperature. Some experimenting with the expression for interpolation was carried out, and the most useful form turned out to be a simple three-parameter exponential, eqn. (45),

$$I(T) = a(1 - b \, \mathrm{e}^{cT}), \tag{45}$$

where a, b and c are fitted parameters, and $I(T)$ is $-\log[\Lambda(T)]$, where $\Lambda(T)$ is one of the phase space integrals in eqns. (43) and (44). The barrier may be calculated as

$$V_{\text{barrier}} = \langle V^{\text{sad}}_{\text{total}} \rangle - \langle V^{\text{vdW}}_{\text{total}} \rangle = \langle E^{\text{sad}} \rangle - \langle E^{\text{vdW}} \rangle - \langle T^{\text{sad}} \rangle + \langle T^{\text{vdW}} \rangle, \tag{46}$$

where the brackets $\langle \cdots \rangle$ denote ensemble averages. The reaction barriers obtained from eqn. (46) are given in Table 1. Rates and barriers were compared with results for the bulk reaction,[13] the gas phase reaction[14] and for the reaction in the presence of one and two water molecules.[10] It should be noted that the rates for one and two water molecules[10] were obtained using variational transition state theory, where no dynamics are introduced.

The rate constant of the S_N2 reaction does not fall off continuously as a function of the cluster size but follows a rather irregular path from the gas-phase value to the value corresponding to the rate constant for the reaction in aqueous solution. A similar pattern holds for the variation of the reaction barrier as a function of the cluster size.

The transmission factor ξ varies slightly with the cluster size but is in general around 1 and does not have any effect on the variation of the rate constant with respect to the cluster size. The transmission factors were all within 0.98 ± 0.01 for all the cluster sizes.

Cluster simulations

A few configurations have also been simulated for much longer than the equilibration time used in calculating the rate constants. These simulations have also been carried out for different cluster sizes with the reactant system in both the vdW configuration, and the sad configuration.

The behavior of water clusters is not as well established as that of liquid water. Some questions regarding stability, structure and dynamical properties can be answered using molecular dynamics simulations. Unfortunately there are difficulties connected with simulations of clusters. As an example, most empirical water potentials are parametrized to model liquid water and one should not expect that they work for clusters. While the gas-phase dipole moment of the water molecule is 1.8 D, most empirical potentials have a dipole moment of 2.5–2.6 D, which corresponds to liquid water. The water dimer has a dipole moment of about 2.2 D, and it should therefore be expected that the dipole moment of a molecule in a cluster is somewhere between 2.2 and 2.6 D. This effect is most conveniently included by using a potential with explicit polarizabilities. It is especially important in the case where the solvation of an ion is considered; the dipole moment of a water molecule in the first solvation shell of the ion has a much different dipole moment than a water molecule in liquid water. From a statistical point of view, cluster simulations are also difficult. Owing to the small number of molecules, it is not easy to obtain well-averaged properties. For this reason most results obtained from MD simulations are given here only for the larger clusters. In addition we discovered that some water molecules have the tendency to leave the clusters – a fact that had to be taken into account when discussing, e.g., diffusion. We compare our

Table 1. Reaction rates and barriers as a function of temperature and cluster size. Energy units are kJ mol^{-1}. Rate units are cm^3 s^{-1}. The notation $x(y)$ means $x \times 10^y$.

	Number of water molecules													
T/K	0	1	2	3	6	9	11	12	14	16	21	30	∞	
290				1.8(−23)	1.1(−21)	8.5(−22)	1.8(−23)	3.8(25)	2.0(−25)	9.9(−24)	2.0(−24)	2.7(−24)		
300	5.0(−15)	1.1(−17)	3.7(−20)	5.3(−23)	4.2(−21)	1.9(−21)	4.4(−23)	1.7(24)	1.2(−24)	4.1(−22)	3.5(−23)	1.4(−23)	3(−30)	
310				1.5(−22)	1.4(−20)	4.3(−21)	1.1(−22)	7.0(24)	6.3(−24)	1.1(−22)	1.0(−23)	7.2(−23)		
320				4.4(−22)	4.5(−20)	9.2(−21)	2.7(−22)	2.8(23)	3.0(−23)	2.6(−22)	2.7(−23)	3.5(−22)		
330				1.2(−21)	1.3(−19)	1.9(−20)	6.5(−22)	1.1(22)	1.3(−22)	6.3(−22)	1.6(−22)	1.6(−21)		
$\langle E_{vdW} \rangle$				−64.8	−80.9	−101.9	−124.2	−138	−168	−156	−216	−367		
$\langle T_{vdW} \rangle$				37.1	74.7	113	133	137	155	184	224	294		
$\langle E_{sad} \rangle$				−0.4	−17.0	−38.8	−62.0	−73.4	−97.6	−106	−148	−305		
$\langle T_{sad} \rangle$				37.1	65.4	89.8	105	113	127	149	199	272		
$\langle V_{barrier} \rangle$	15	25	45	64	73	86	90	89	98	85	93	84	99	

results with those obtained for simulation of the same reactant system in the bulk liquid.[25]

Structure. Structural aspects of the water clusters have been examined by calculating radial distribution functions. When calculating radial distribution functions (RDFs), the function is usually normalized against the number density in an ideal gas at the same density.[26] When dealing with clusters the density is not as well defined as in a bulk liquid. In this work we therefore normalized all RDFs against an ideal gas with the density 1.00 g cm^{-3}. All 11 possible RDFs were calculated for different cluster sizes. The Cl–O RDF is shown in Fig. 2. First of all we note the strong coordination of water to the chloride ion in the vdW simulations (the chlorine denoted Cl_1). We note further that the polarized sad complex is also able to coordinate water molecules fairly strongly, although the sharpness of the first peak in the Cl_1–H RDF (Fig. 3) suggests a stronger coordination to the chloride ion. The water molecules (denoted wms) are divided into four groups from the Cl_1–O RDF. This distribution function shows peaks from 0 to 4 Å and from 4 to 7 Å. The division of the interval from 7.0 Å to ∞ has been done in order to put the departed wms in a separate group No. 4. The value of 22.0 Å was chosen because we found that molecules that moved further away than this did not return to the cluster later. Thus, the molecules belonging to the fourth group have been separated from the cluster. It was found for most simulations that no water molecule would enter group 4 after about 25 ps, but in some simulations departures could occur after about 50 ps. Other simulations at lower temperatures do not exhibit this behavior. The reason for choosing a temperature range around 300 K was to enable the comparison of the rate constants with the results for bulk water. It is very likely that in experiments the cluster temperature will be much lower,[27] and that this instability of the clusters is merely a consequence of our choice of temperature range. This will be investigated in the future.

The difference in the intensity of the first peaks for the 21 wms and the 30 wms simulation is due to the greater number of water molecules in the inner groups for the 30 wms simulation. The Cl–H function is shown in Figs. 3 and 4. It is clear from these figures that the stronger coordination of water to the vdW complex manifests itself in a more intense peak but also a broader peak than obtained from the reactant system in liquid water.[25] This indicates a looser coordination in the cluster than in the liquid phase. Upon examining the Cl_1–O and the Cl–H RDF we see that the peak from the second solvation shell is more intense for vdW than for sad when looking at the larger cluster. However, nearly all intensity is included in the first peak in vdW for the 6 wms simulation, which is not the case for the sad 6 wms simulation. Owing to the lack of an extensive water structure in the small clusters, it is observed that the presence of chloride ion can cause the formation of a thick first solvation shell, rather than – as in the liquid phase – a first and second shell.

In the 6 wms simulation, the peaks of the sad RDFs are positioned at 2.9 and 3.1 Å for chlorine atoms 3 and 1, respectively (the difference is due to the unfavorable statistics) and at 2.9 Å for chlorine number 1 for vdW. In the 30 wms simulation the positions of the peaks are shifted inwards; the sad peaks are both at 2.8 Å and the

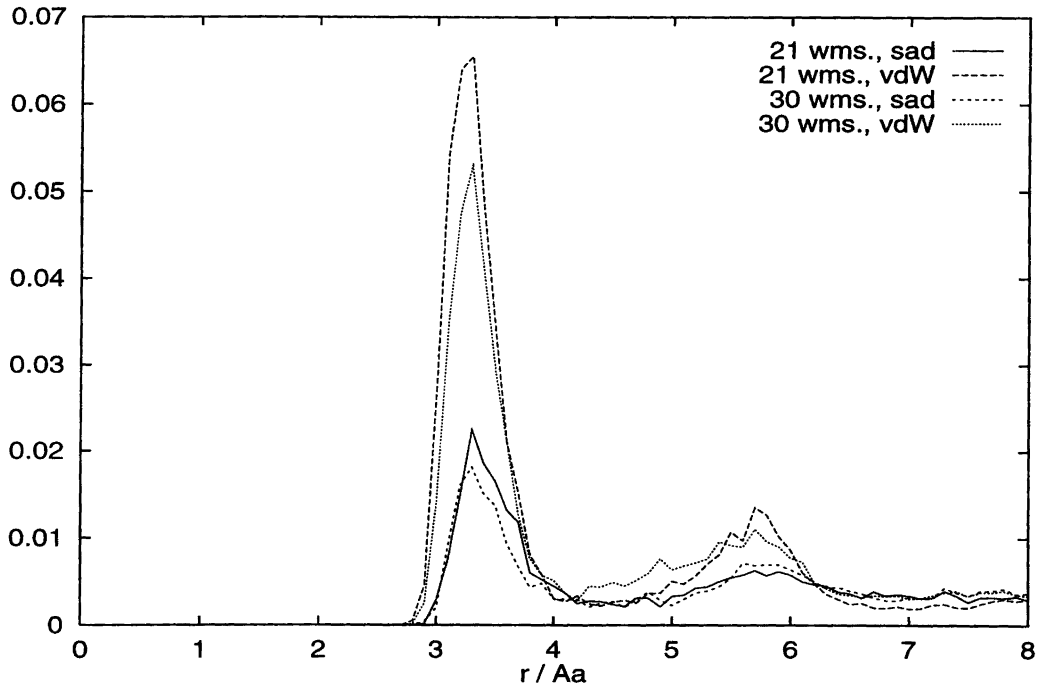

Fig. 2. The Cl_1–O RDF for sad and vdW in the simulations using 21 and 30 water molecules.

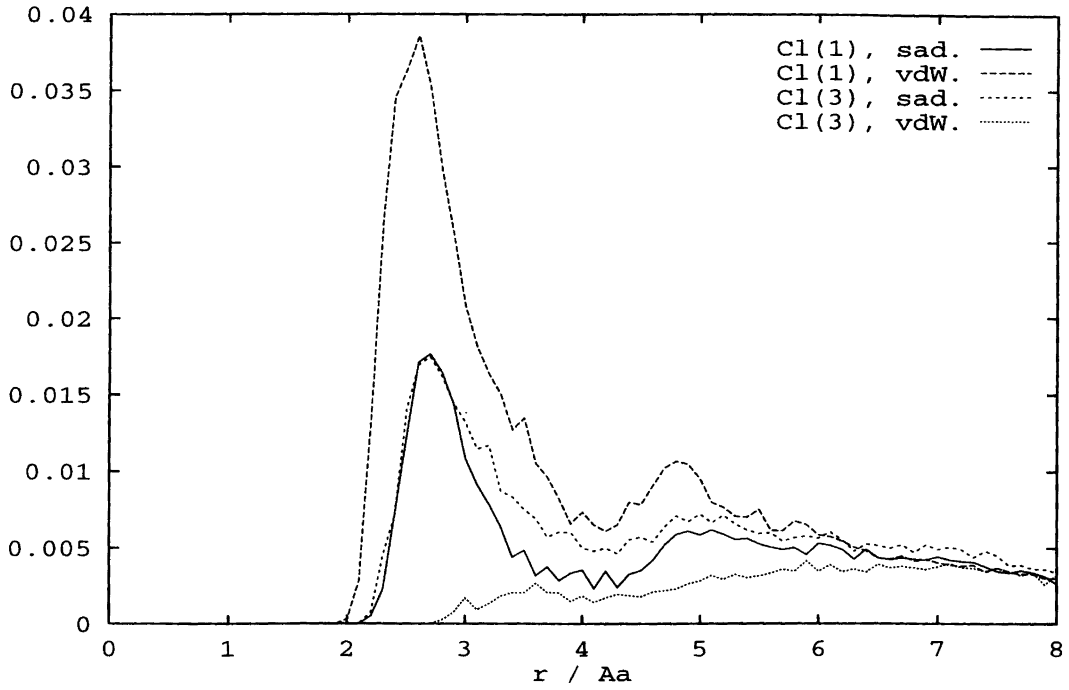

Fig. 3. The Cl–H RDF for sad and vdW with 30 water molecules.

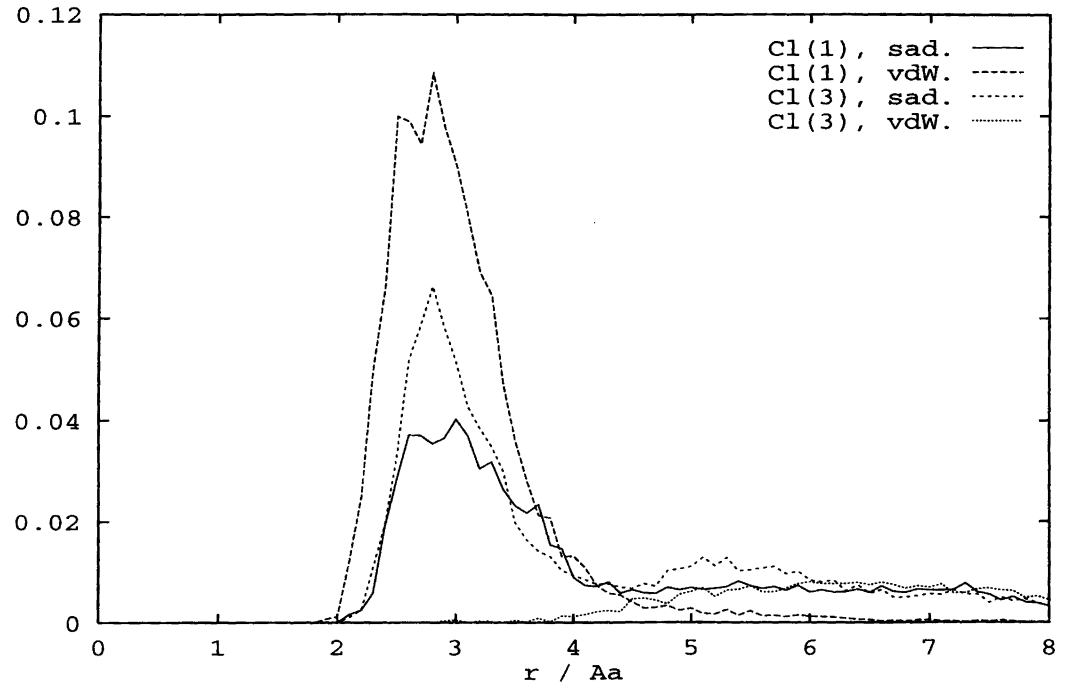

Fig. 4. The Cl–H RDF for sad and vdW with 6 water molecules.

vdW peak is at 2.7 Å. In the water simulation these peaks appear at about 2.2 and 2.3 Å, vdW and sad, respectively. We note a tighter coordination as we move along from 6 to 30 wms and finally to the liquid phase.

Since the chlorine atoms in the sad configuration are equal, we should expect the Cl–H RDF's (Figs. 3 and 4) to be the same no matter which chlorine atom is used for the calculation. We see, however, that this is not the case. This is due to the difficulties regarding statistics which have already been mentioned. It should be noted nevertheless that this is also a problem in liquid simulations.[25]

The partitioning of water molecules into groups is given in Table 2. The distribution of H_2O in the different groups for different cluster sizes is given in Table 3. These numbers confirm the stronger coordination of water to

Table 2. Partitioning of the water molecules into groups.

Group number	Lower limit of r_{OCl_1}/Å	Upper limit of r_{OCl_1}/Å
1	0.0	4.0
2	4.0	7.0
3	7.0	22.0
4	22.0	∞

Table 3. Distribution of water molecules in various groups. The numbers in parentheses are standard deviations on the last decimal, e.g., 0.26(4) means 0.26 with a standard deviation of 4×10^{-2}.

Conf. and cluster size		Number in group 1	2	3	4
sad	3	0.26(4)	0.80(5)	1.25(5)	0.70(5)
	6	0.95(4)	1.50(8)	2.3(1)	1.26(6)
	9	1.30(5)	2.3(1)	4.1(1)	1.35(6)
	12	1.63(5)	2.8(1)	5.9(2)	1.6(1)
	16	1.63(5)	3.0(2)	7.8(2)	3.6(2)
	21	1.29(5)	3.4(2)	10.0(2)	6.3(2)
	30	1.52(8)	4.9(4)	17.5(4)	6.0(3)
vdW	3	1.28(2)	0.75(3)	0.03(2)	0.93(3)
	6	2.28(5)	0.69(5)	0.21(8)	2.81(7)
	9	2.74(7)	2.44(8)	1.5(1)	2.3(1)
	12	3.28(6)	3.41(9)	3.2(2)	2.1(2)
	16	2.97(5)	3.36(8)	3.9(2)	5.8(2)
	21	3.49(7)	4.3(1)	5.3(2)	7.9(2)
	30	3.93(9)	6.9(3)	12.7(4)	6.4(3)

the vdW complex. We note that the vdW complex can coordinate at least 3.9 water molecules in the first group (corresponding to the first solvation shell in the cluster), whereas for the first group of the sad complex we note a saturation of about 1.5 water molecules. Note that no saturation is observed for vdW. There is also a tendency towards filling the vdW groups from the inside that is not observed for the sad complex; note how the fraction of molecules in the first vdW group decreases with increasing cluster size. By associating the integral of the peak in the Cl_1–O RDF from 0–4.0 Å with the number of molecules in group 1, we can, despite the problem with normalization of the RDFs, use this association to obtain coordination numbers from the integrals. The two sad peaks in the Cl_3–O RDF obtained from the 30 wms simulation can, in this way be integrated to about 2 and 6 wms for the first and second peak, respectively. These numbers should be compared with the numbers in Table 3 for the number of molecules belonging to groups 1 and 2 which are 1.52 and 4.9, respectively. The observed difference is due to the unfavorable statistics.

Dynamical properties. Translational diffusion coefficients without contamination of cluster translation and rotation were calculated using the long time limit of the mean square displacement as shown in eqn. (47)[26]

$$D = \lim_{t\to\infty} \langle [\boldsymbol{r}(t) \cdot \boldsymbol{r}(0)]^2 \rangle / 6t \qquad (47)$$

Table 4. Diffusion coefficients. Units are $10^{-8}\ m^2\ s^{-1}$. The second set of numbers use only the simulation time during which no water molecules depart to group 4. The numbers in parentheses are standard deviations on the last decimal.

	sad, 0–60 ps	vdW, 0–60 ps
30 water molecules		
Total	1.9(3)	1.8(3)
Group 1	0.9(3)	1.1(1)
Group 2	1.33(8)	1.5(1)
Group 3	2.1(4)	2.2(5)
	sad, 20–60 ps	vdW, 14–60 ps
Total	1.4(1)	1.5(2)
Group 1	0.9(3)	1.08(9)
Group 2	1.18(8)	1.28(9)
Group 3	1.5(2)	1.9(4)
	sad, 0–80 ps	vdW, 0–80 ps
21 Water molecules		
Total	1.9(4)	1.7(2)
Group 1	1.05(3)	1.0(2)
Group 2	1.35(8)	1.6(3)
Group 3	2.2(5)	2.2(5)
	sad, 14–80 ps	vdW, 26–80 ps
Total	1.5(2)	1.4(2)
Group 1	1.02(2)	1.0(1)
Group 2	1.19(8)	1.6(3)
Group 3	1.6(5)	1.4(5)

and are presented in Table 4. In the calculation of the diffusion coefficient from eqn. (47), the free water molecules in group 4 give a quadratic contribution to the ensemble average. These molecules are therefore excluded in the calculation owing to their non-diffusive motion. Furthermore, it is necessary to wait until the final water molecule has departed to group 4, in order to avoid their contribution to the diffusion coefficient on their way out, which is also a non-diffusive contribution. Omitting to wait for the wms to leave results in a difference in the diffusion coefficients, as seen in Table 4; we observe less diffusion when using only the last part of the simulations. In some simulations a tendency to non-diffusive motion is also seen in group 3. The molecules far away from the reactant system tend to move much more freely than molecules in liquid water. We observe, from the values of the diffusion coefficients, that the molecules in general move faster than in a liquid. These values are almost an order of magnitude greater than diffusion coefficients for water.[28] We should of course bear in mind that the non-diffusive behavior of water in the outer group of course shifts the diffusion coefficients upwards.

We note further that diffusion increases as we move from group 1 to group 3. This is what should be expected since the water molecules will be more tightly coordinated in the inner group than in the outer. We did not, however, notice any significant differences in the numbers for vdW and sad, which is not what one would expect in a liquid simulation. The wms close to the chloride ion would be

expected to move less than the molecules close to the polarized sad system. One possible explanation for this could be that, owing to the low density of wms in the cluster, the molecules close to the chloride ion are not able to donate the kinetic energy gained from descending the potential surface. They are therefore not able to stay close to the chloride ion long enough to give rise to a low diffusion coefficient for the innermost group.

Different auto-correlation functions of water properties were calculated. The function

$$C_{ii}(t) = \langle \boldsymbol{i}(0) \cdot \boldsymbol{i}(t) \rangle \tag{48}$$

was calculated for three different vectors, namely $C_{dd}(t)$, $C_{hh}(t)$ and $C_{oo}(t)$. The vectors these functions refer to are $\boldsymbol{d}$ – the water dipole vector that is parallel to the C_2 axis in the molecule, $\boldsymbol{h}$ – the vector parallel to the vector connecting the hydrogen atoms in water, and $\boldsymbol{o}$ – the vector orthogonal to $\boldsymbol{d}$ and $\boldsymbol{h}$ (out-of-plane). We considered how the orientational decay occurs and we present in Table 5 the orientational decay times. The decay times should be compared to the numbers in the same table obtained for liquid water.[2,3] We found that the decay times are about 3–4 times shorter than for liquid water, which also indicates a less tightly coordinated structure than liquid water. The dipole vector does, although, relax still more slowly than the hydrogen and out-of-plane vectors, as in the liquid.

Table 5. Orientational decay times for water in the different groups in the calculations using 30 water molecules. Units are ps.

Axes	Group 1	Group 2	Group 3	Groups 1–3
vdW using 14–50 ps simulation time				
Dipole	3.8	3.1	2.3	3.1
H–H	0.25	0.82	0.35	0.53
Out-of-plane	0.26	0.67	0.40	0.48
sad using 14–50 ps simulation time				
Dipole	3.8	3.3	3.0	3.2
H–H	0.27	0.56	0.70	0.60
Out-of-plane	0.26	0.55	0.59	0.58
Axes	Wallqvist[2]		Åstrand[3]	
Liquid water				
Dipole	10.2		13.9	
H–H	9.8		10.4	
Out-of-plane	7.6		10.1	

The translational kinetic temperature, T_{kin}, was calculated for the different groups. The result is given in Table 6. It is seen that T_{kin} tends to decrease as we go from group 1 to group 3 when looking at vdW calculations. This tendency is not present in the sad results. This confirms that the wms close to the chloride ion gain kinetic energy which cannot easily be lost in collisions with neighboring molecules owing to the low density, as discussed earlier. We also note that the precision of the kinetic temperature improves as we move from group 1 to 3 as a consequence of the better statistics in the group containing the bulk of the wms. The distribution of the lifetimes within the different groups was also calculated. The result can be seen in Table 7. First of all note that this distribution does not change significantly when the first part of the simulation is discarded. Since the size of the cluster increases during the first part of the simulation during the relaxation of the liquid structure, this might have been expected. We note that all distributions are dominated by short visits in the interval 0.0–0.5 ps. The visit length decays in an exponential-like manner, but no decay times were calculated owing to the unfavorable statistics. When comparing the numbers for group 1 for sad and vdW, we see that for sad, the very short visits constitute more than half the number of total visits, whereas for vdW they contribute less than one third. This shows that the water molecules tend to stay longer near the charged ion, than the polarized complex. The difference is however, not large enough to change the other dynamical properties, as already mentioned. When comparing groups 2 and 3 for sad and vdW, we see that the visit lengths are similar. In addition very long lifetimes are encountered most frequently in group 3 for both sad and vdW, as would be expected owing to the fact that the molecules belonging to this group can occupy a large region in space compared with groups 1 and 2.

Conclusions

The water molecules tend to remain longer near the charged ion than the polarized complex. This difference though is not large enough to change the other dynamical properties. When comparing groups 2 and 3 for sad and vdW we see that the visit lengths are similar. We observe

Table 6. Translational kinetic temperatures in the different groups. Units are *K*. The numbers in parentheses are standard deviations on the last decimal.

		Group					
N_w[a]	Type	1	2	3	4	1–3	Total
30	vdW	308(8)	294(6)	291(4)	$2.8(2) \times 10^2$	295(3)	290(3)
	sad	$3.0(1) \times 10^2$	298(8)	283(3)	$2.6(2) \times 10^2$	287(3)	286(4)
21	vdW	279(9)	262(8)	241(7)	335(7)	257(6)	294(3)
	sad	$2.4(1) \times 10^2$	253(8)	266(6)	214(6)	265(5)	255(4)

[a]The number of water molecules in the cluster.

Table 7. The distribution of visit lengths in the various groups. Units are ps.

Time interval	vdW			sad		
0.0–0.5	0.29	0.52	0.29	0.57	0.43	0.27
0.5–1.0	0.16	0.15	0.20	0.14	0.19	0.11
1.0–1.5	0.11	0.08	0.10	0.06	0.11	0.08
1.5–2.0	0.10	0.04	0.07	0.08	0.08	0.05
2.0–2.5	0.06	0.04	0.02	0.0	0.04	0.02
2.5–3.0	0.07	0.03	0.02	0.02	0.02	0.03
3.0–3.5	0.06	0.02	0.04	0.02	0.02	0.02
3.5–4.0	0.03	0.02	0.008	0.02	0.006	0.04
4.0–4.5	0.04	0.02	0.008	0.02	0.02	0.02
4.5–5.0	0.01	0.0	0.04	0.0	0.02	0.03
5.0–∞	0.07	0.07	0.19	0.06	0.05	0.34
N_{vis}[a]	89	214	127	49	178	132

[a] The number of visits in each group in each simulation.

that the wms close to the chloride ion gain kinetic energy, an energy that is not easily lost in the collisions with neighboring molecules, owing to the low density. Comparisons with liquid water show that the clusters do not have tightly coordinated structures like those in liquid water. The low density of wms in the cluster might be an explanation for this since the molecules close to the chloride ion are not able to transfer their kinetic energy to the surrounding solvent molecules. We note that the vdW complex coordinates a larger proportion of water molecules in the first group compared with that of the sad complex and that, not surprisingly, the fraction of molecules in the first vdW group decreases with increasing cluster size.

The variation of the barrier with cluster size relates to the relative stabilization of the van der Waals complex and the transition state complex. We observe from Table 3 that the clusters with large reaction barriers are those for which the van der Waal complex is more tightly bound by the water molecules than the transition state complex. Table 1 shows the irregularities of the rate constants for clusters of 3, 12 and 14 water molecules. In Table 3 we observe that for these clusters the van der Waal complex is more tightly solvated, as seen from the relatively large number of water molecules in group 1 compared with the number of corresponding water molecules around the transition state complex. This leads to stronger solvation shells around the van der Waal complex than around the transition state complex and therefore larger reaction barriers.

Acknowledgements. K.V.M. thanks *Statens Naturvidenskabelige Forskningsråd* for support. K.V.M. also thanks Professor H. Lund for his inspiring ideas within the field of electron transfer.

References

1. Shaik, S. S., Schlegel, H. B. and Wolfe, S. *Theoretical Aspects of Physical Organic Chemistry: The S_N2 Mechanism*, Wiley, New York 1992.
2. Wallqvist, A., Ahlström, P. and Karlström, G. *J. Phys. Chem. 94* (1990) 1649; erratum in *J. Phys. Chem. 95* (1991) 4922.
3. Åstrand, P. O., Linse, P. and Karlström, G. *Chem. Phys. 191* (1995) 195.
4. Bunton, C. A. *Nuceophilic Substitution at a Saturated Carbon Atom*, Elsevier, Amsterdam 1963.
5. Ingold, C. K. *Structure and Mechanism in Organic Chemistry*, Cornell University Press, NY 1969.
6. Bentley, T. W. and Schleyer, P. v. R. *Adv. Phys. Org. Chem. 14* (1977) 14.
7. Hughes, E. D., Ingold, C. K. and Patel, C. S. *J. Chem. Soc. 526* (1933).
8. Gleave, J. L., Hughes, E. D. and Ingold, C. K. *J. Chem. Soc. 236* (1935).
9. Lund, H., Daasbjerg, K., Lund, T. and Pedersen, S. U. *Acc. Chem. Res. 28* (1995) 313.
10. Tucker, S. C. and Truhlar, D. G. *J. Am. Chem. Soc. 112* (1990) 3338.
11. Tucker, S. C. and Truhlar, D. G. *J. Am. Chem. Soc. 112* (1990) 3347.
12. Linde, S. V. V. and Hase, W. L. *J. Am. Chem. Soc. 111* (1989) 2349.
13. Billing, G. D. and Mikkelsen, K. V. *Chem. Phys. 182* (1994) 249.
14. Billing, G. D. *Chem. Phys. 159* (1992) 109.
15. Prigogine, I. and Rice, S. A. *Adv. Chem. Phys. 70* (1988) 1.
16. McQuarrie, D. A. *Statistical Mechanics*, Harper Collins, New York 1976.
17. Billing, G. D. and Mikkelsen, K. V. *Introduction to Molecular Dynamics and Chemical Kinetics*, Wiley, New York 1996.
18. Anderson, J. B. *J. Chem. Phys. 58* (1973) 4684.
19. Jaffe, R. L., Henry, J. M. and Anderson, J. B. *J. Chem. Phys. 59* (1973) 1128.
20. Ahlström, P., Wallqvist, A., Engström, S. and Jönsson, B. *Mol. Phys. 68* (1989) 563.
21. Kistenmacher, H., Popkie, H. and Clementi, E. *J. Chem. Phys. 59* (1973) 5842.
22. Clementi, E., Cavallone, F. and Scordamaglia, R. *J. Am. Chem. Soc. 99* (1977) 5531.
23. Linse, P. and Wallqvist, A. MOLSIM 1.2, Lund University, Sweden 1991.
24. Metropolis, N., Rosenbluth, A. W., Rosenbluth, M. N., Teller, A. H. and Teller, E. *J. Chem. Phys. 21* (1953) 1087.
25. Chandrasekhar, J., Smith, S. F. and Jorgensen, W. L. *J. Am. Chem. Soc. 107* (1988) 154.
26. Allen, M. P. and Tildesley, D. S. *Computer Simulations of Liquids*, Clarendon, Oxford 1987.
27. Fluendy, M. A. D. and Lawley, K. P. *Chemical Applications of Molecular Beam Scattering*, Chapman and Hall, London 1973.
28. Jorgensen, W. L., Chandrasekhar, J., Madura, J. D., Impey, R. W. and Klein, M. L. *J. Chem. Phys. 79* (1983) 926.

Received February 18, 1999.